



A Catalog of Cool Dwarf Targets for the *Transiting Exoplanet Survey Satellite*

Philip S. Muirhead¹, Courtney D. Dressing², Andrew W. Mann^{3,9}, Bárbara Rojas-Ayala⁴, Sébastien Lépine⁵,
Martin Paegert⁶, Nathan De Lee^{7,8}, and Ryan Oelkers⁸

¹ Department of Astronomy, ² Institute for Astrophysical Research, Boston University, 725 Commonwealth Avenue, Boston, MA 02215, USA

² Department of Astronomy, The University of California, Berkeley, CA 94720, USA

³ Department of Astronomy, The University of Texas at Austin, Austin, TX 78712, USA

⁴ Departamento de Ciencias Físicas, Universidad Andres Bello, Fernandez Concha 700, Las Condes, Santiago, Chile

⁵ Department of Physics and Astronomy, Georgia State University, Atlanta, GA 30303, USA

⁶ Harvard-Smithsonian Center for Astrophysics, 60 Garden St, Cambridge, MA 02138, USA

⁷ Department of Physics, Geology and Engineering Tech, Northern Kentucky University, Highland Heights, KY 41099, USA

⁸ Department of Physics & Astronomy, Vanderbilt University, 6301 Stevenson Center Ln., Nashville, TN 37235, USA; philipm@bu.edu

Received 2017 September 21; revised 2018 February 10; accepted 2018 February 19; published 2018 April 3

Abstract

We present a catalog of cool dwarf targets ($V - J > 2.7$, $T_{\text{eff}} \lesssim 4000$ K) and their stellar properties for the upcoming *Transiting Exoplanet Survey Satellite* (*TESS*), for the purpose of determining which cool dwarfs should be observed using two minute observations. *TESS* has the opportunity to search tens of thousands of nearby, cool, late K- and M-type dwarfs for transiting exoplanets, an order of magnitude more than current or previous transiting exoplanet surveys, such as *Kepler*, *K2*, and ground-based programs. This necessitates a new approach to choosing cool dwarf targets. Cool dwarfs are chosen by collating parallax and proper motion catalogs from the literature and subjecting them to a variety of selection criteria. We calculate stellar parameters and *TESS* magnitudes using the best possible relations from the literature while maintaining uniformity of methods for the sake of reproducibility. We estimate the expected planet yield from *TESS* observations using statistical results from the *Kepler* mission, and use these results to choose the best targets for two minute observations, optimizing for small planets for which masses can conceivably be measured using follow-up Doppler spectroscopy by current and future Doppler spectrometers. The catalog is available in machine readable format and is incorporated into the *TESS* Input Catalog and *TESS* Candidate Target List until a more complete and accurate cool dwarf catalog identified by ESA's *Gaia* mission can be incorporated.

Key words: planetary systems – stars: fundamental parameters – stars: late-type – stars: low-mass

Supporting material: machine-readable table

1. Introduction

Cool dwarf stars, specifically late K dwarf and M dwarf stars, are exciting targets for exoplanet surveys. Compared to Sun-like and earlier-type dwarfs, the smaller masses and radii of cool dwarf stars enable the detection and characterizing of smaller and less-massive exoplanets via the transit and radial velocity techniques (e.g., Nutzman & Charbonneau 2008; Muirhead et al. 2011). For these reasons, some of the smallest exoplanets found to date orbit cool dwarf stars, including sub-Earth-sized exoplanets, such as Kepler-1308 b ($0.51 R_{\oplus}$), Kepler-138 b ($0.52 R_{\oplus}$, both from Morton et al. 2016), *K2*-89 b ($0.62 R_{\oplus}$, Crossfield et al. 2016), and Kepler-42 c ($0.73 R_{\oplus}$, Muirhead et al. 2012; Mann et al. 2017). Planets orbiting within cool dwarf stars' habitable zones are more easily discovered than those orbiting within the habitable zones of Sun-like stars. Moreover, potentially habitable exoplanets orbiting cool dwarfs are more easily characterized via transit transmission spectroscopy, thanks to the increased number of transits in a given amount of time and the relatively deep transit signals from terrestrial-size planets (Kaltenegger & Traub 2009; Belu et al. 2011). In fact, a recent study by Kane et al. (2016) found that of all the planet candidates discovered by NASA's *Kepler* mission that are less than $2.0 R_{\oplus}$ and reside within an optimistically sized habitable zone, 40% orbit stars with effective temperatures of less than 4000 K. This is despite the

fact that cool dwarfs make up less than 5% of the initial *Kepler* target sample (Batalha et al. 2010). Investigations of planets orbiting M dwarfs show that the majority of M dwarfs host more than two planets with periods of less than 200 days (e.g., Dressing & Charbonneau 2013; Gaidos et al. 2014), that one in five mid-M dwarfs hosts compact multiple systems (Muirhead et al. 2015), and that one in seven M dwarfs hosts an Earth-sized planet orbiting within the habitable zone (Dressing & Charbonneau 2015).

Because they both outnumber and are intrinsically fainter than Sun-like stars, bright ($J < 12$) cool dwarfs tend to be more evenly distributed across the sky, rather than concentrated toward the Galactic plane. For this reason, NASA's *Kepler* and *K2* missions can only observe a few thousand cool dwarf stars continuously for transiting exoplanets. Ground-based transit programs, such as M_{Earth} (e.g., Berta et al. 2013) and TRAPPIST (e.g., Gillon et al. 2012) monitor the brightest and nearest cool dwarfs by individually targeting them one at a time. However, these programs suffer from noise associated with ground-based precision photometry and diurnal and weather-induced time-coverage challenges, similarly limiting their target lists to hundreds or thousands. In contrast, NASA's upcoming *Transiting Exoplanet Survey Satellite* (*TESS*) is uniquely suited to search an order of magnitude more cool dwarfs for transiting exoplanets by utilizing wide-angle imaging cameras in a space environment.

Ricker (2014) provided a detailed description of the observing mode of *TESS*. Similar to *Kepler*, *TESS* will have

⁹ Hubble Fellow.

a “two minute” observing mode, wherein two minute exposures are acquired for a limited number of apertures in the *TESS* fields. So-called “full-frame” observations, consisting of 30 minute exposures, are acquired for the entirety of each *TESS* field. The apertures chosen for two minute observations require careful consideration. (Sullivan et al. 2015, hereafter S15) first calculated the number of stars of various spectral types that *TESS* could observe with two minute observations in order to maximize the number of planet discoveries, using statistics from prior exoplanet surveys. They showed that, optimally, *TESS* would observe roughly 50,000 stars with effective temperatures less than 4000 K and *TESS* magnitudes brighter than 16, and should detect roughly 500 transiting planets orbiting those stars.

However, S15 did not use literature star catalogs in their simulation. Instead, they used galactic models to simulate observable stars. Determining the actual 50,000 cool dwarf stars that *TESS* should observe is itself a challenge. By far the most reliable method for identifying individual cool dwarfs is with archival trigonometric parallax observations via mass–luminosity relations. Trigonometric parallax measurements provide absolute magnitudes for stars, and absolute infrared magnitude has been shown to determine star mass with no perceivable effect from stellar metallicity (e.g., Henry & McCarthy 1993; Henry et al. 1999; Delfosse et al. 2000; Boyajian et al. 2012; Mann et al. 2013b; Benedict et al. 2016). Unfortunately, archival trigonometric parallax measurements for stars, such as those measured by the *Hipparcos* mission (van Leeuwen 2007), do not include significant numbers of cool dwarfs due to their intrinsic faintness. Soon, ESA’s *Gaia* mission will measure trigonometric parallaxes for hundreds of thousands of cool dwarfs, and those measurements will be enormously useful for deciding the *TESS* targets appropriate for two minute cadence. In the meantime, however, *TESS* cool dwarf targets must be chosen by other means.

In the absence of trigonometric parallaxes, cool dwarfs must be selected using archival spectroscopic, color and/or proper motion measurements. In this paper, we describe a catalog of cool dwarfs for two minute *TESS* observations using archival parallaxes where available, or proper motion observations from the SUPERBLINK program (Lépine & Gaidos 2011), in combination with a variety of photometric catalogs. In Section 2 we discuss our methods for identifying cool dwarf stars, and in Section 3 we compare the expected planet yields for *TESS* observations of real stars to those of S15. In Section 4 we discuss the importance of this catalog of cool dwarfs for *TESS* discoveries and follow-up observations.

2. Methods

2.1. Catalogs

Despite the emergence of high-volume, large-scale sky surveys, all-sky star catalogs that include tens of thousands of bright cool dwarfs are surprisingly rare. Spectroscopic surveys either do not contain the necessary number of cool dwarfs to meet the simulations from S15, or the stars in the catalogs are too faint to be good *TESS* targets ($I_C > 15$). West et al. (2008) presented over 70,000 M dwarfs spectroscopically verified from the Sloan Digital Sky Survey (SDSS); however the fields observed by the SDSS are limited to specific regions of the sky with visible-band magnitudes greater than 15. The same is true for cool dwarfs with spectra measured by LAMOST (Yi et al. 2014). S15 calculated

that cool dwarfs fainter than 15th magnitude in the *I*-band are not ideal for *TESS* observations due to the significant role of photon noise.

On the other hand, *targeted* spectroscopic surveys of nearby cool dwarfs, such as the Palomar/Michigan State University (PMSU) Survey (Reid et al. 1995, 2002; Hawley et al. 1997; Gizis et al. 2002) are nearly all sky, but only include hundreds of cool dwarfs. More recently, cool dwarf spectroscopic surveys by Rojas-Ayala et al. (2012), Deshpande et al. (2013), Newton et al. (2014), Terrien et al. (2015), and Zhong et al. (2015) have increased the number of spectroscopically characterized bright cool dwarfs. However, together, these spectroscopic surveys have characterized only about 2000 cool dwarfs, not the tens of thousands needed to optimally assign two minute apertures for *TESS* observations.

In order to acquire tens of thousands of cool dwarfs with *TESS* magnitudes brighter than T of 16, we must turn to photometric surveys and select objects based on broadband colors alone. The Two-Micron All-Sky Survey (2MASS; Cutri et al. 2003; Skrutskie et al. 2006) provides J -, H -, and K_s -band magnitudes for nearly all stars that *TESS* can observe for transiting planets. J -, H -, and K_s -band colors provide some information on the properties of stars, and can be effectively used for isolating late M dwarfs from earlier-type stars and, in some cases, evolved stars. However, on their own J -, H -, and K_s -band colors are of limited use for identifying late K or early M dwarf stars, due to their significant overlap with evolved stars (see for example Bessell & Brett 1988, their Figure 5) and with earlier-type stars suffering moderate amounts of interstellar reddening. Similarly, the *Wide-field Infrared Survey Satellite* (*WISE*) provides mid-infrared magnitudes for the entire sky, although for typical M dwarf temperatures, there is little difference between 2MASS and *WISE* magnitudes, both bands being on the Rayleigh–Jeans side of the Planck law corresponding to these effective temperatures.

The best method to identify M dwarfs in photometric surveys is to include proper motion data. Stars with moderately large proper motions ($>20 \text{ mas yr}^{-1}$) tend to be relatively nearby, and this presents two advantages. On the one hand, red giants and red dwarfs have large ($\gtrsim 5 \text{ mag}$) absolute magnitude differences, and giants can thus be easily identified in samples of high proper motion stars, as they are systematically brighter. On the other hand, stars with large proper motions are also relatively nearby ($d < 1 \text{ kpc}$) and thus unlikely to suffer significant amounts of reddening. As a result, samples of stars with large proper motions are generally dominated by nearby K and M dwarfs, and their effective temperatures can be estimated with some certainty based on broadband, optical-to-infrared colors.

The SUPERBLINK proper motion catalog (S. Lépine 2018, in preparation), is an all-sky catalog of stars with large proper motions ($\mu > 40 \text{ mas yr}^{-1}$) which includes optical and infrared magnitudes for all its entries. These include optical G -band magnitudes from the first *Gaia* release, whenever available, and estimated optical V -band magnitudes for all the stars. The SUPERBLINK survey is based out of a project to identify all high proper motion stars from archival plates from the Digitized Sky Surveys. SUPERBLINK uses, for example, images from the National Geographic Palomar Observatory Sky Survey (POSS I; Minkowski & Abell 1963) and the Second Palomar Observatory Sky Survey (POSS II, conducted roughly 40 years later; Reid et al. 1991). Both surveys were

originally performed using photograph plates, and both have since been digitized (Djorgovski et al. 2002; Gal et al. 2004; Odewahn et al. 2004), enabling computation methods for identifying high proper motion objects.

Instead of directly measuring stellar positions, SUPERBLINK use an image-differencing algorithm, which identifies moving objects from their patterns of residuals after image subtraction. As a result, the method works successfully in crowded fields of low Galactic latitudes (see e.g., Lépine et al. 2002). In addition, the SUPERBLINK survey includes stringent quality control tests, and all but the most obvious detections are individually examined by eye, on the computer screen, using a blink-comparator widget. Additional processing includes cross-correlation with several photometric catalogs, including *GALEX*, SDSS, USNO-B1.0, *Gaia* DR1, 2MASS, and *WISE*. The proper identification of the counterparts of these high proper motion stars at all the various epochs of those catalogs is made easy by the prior knowledge of their proper motion vectors.

In addition to image-differenced proper motions, SUPERBLINK incorporates positions and proper motions from *Gaia* DR1 where available (Gaia Collaboration et al. 2016a, 2016b). The *Gaia* proper motions are labelled `_new` in the SUPERBLINK catalog and the Cool Dwarf Catalog (CDC).

As a base catalog for determining cool dwarfs for *TESS* observations, we therefore adopted the SUPERBLINK catalog as the primary source of targets. Although SUPERBLINK already lists 2MASS magnitudes for most objects, we independently cross-matched the catalog again with 2MASS in order to obtain the 2MASS photometric flags.

SUPERBLINK contains Tycho-2 V -band magnitudes where available (Høg et al. 2000). More recent visible magnitudes are available from the American Association Variable Star Observers Photometric All-sky Survey (APASS, Henden & Munari 2014) catalog. APASS contains Landolt B and V magnitudes, and SDSS-like g' , r' and i' magnitudes for roughly 2.5 million stars. We therefore cross-matched SUPERBLINK with APASS in addition to 2MASS.

Cross-matching between the three catalogs was performed using a PostgreSQL database maintained at Vanderbilt University for the purpose of determining the *TESS* Input Catalog and the Candidate Target List (TIC and CTL; Stassun et al. 2017). The SQL database contains complete catalogs, which we cross-matched and filtered using an SQL query. The resulting cross-matched catalog contained 2704,792 entries.

2.2. Determining a Visible-band Magnitude

As stated in the previous section, at least one visible-band magnitude provides a significant constraint on M dwarf effective temperatures. We chose to use the Johnson V -band owing to its wide availability. For the SUPERBLINK/2MASS/APASS cross-matched catalog, we determined the best V -band magnitude based on the perceived reliability of APASS, Tycho-2, and the V -magnitude estimated in SUPERBLINK, called V_T . If APASS V was available with 1σ uncertainties of less than 0.1 mag, we chose that as the V -band magnitude. If, however, APASS was not available or had 1σ uncertainties larger than 0.1 mag, then we chose the Tycho-2 magnitude and assigned an uncertainty of either 0.013 or 0.1 mag, for $V < 9.0$ and $V \geq 9.0$ respectively, following Høg et al. (2000). If the Tycho-2 magnitude was not available, we chose the SUPERBLINK V_T magnitude, an estimate of the

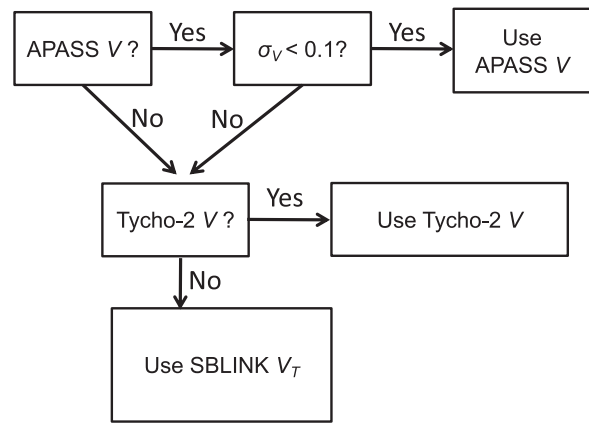


Figure 1. Decision chart indicating which archival measurement is used to determine a V -band magnitude for a given object in SUPERBLINK.

star’s V -band magnitude based on scanned plates. The V_T magnitude is described in Lépine & Gaidos (2011) and includes an estimate of the uncertainty. Figure 1 describes the process of choosing a V -band magnitude for each star.

With this V -band magnitude in hand, we applied criteria to isolate cool stars from stars with Sun-like and hotter photospheric temperatures. As a primary criterion for identifying cool dwarfs, we selected only stars with $V - J > 2.7$, as suggested in Lépine & Gaidos (2011). As demonstrated in Lépine et al. (2013), this selection should include nearly all dwarfs of subtype M0 and later, with only some contamination from late-type K dwarfs. However, unlike Lépine & Gaidos (2011), we do not apply a brightness cut of $J < 10$, in order to increase the number of stars in the catalog to a value closer to that predicted in S15, at the expense of perhaps including a few M giant contaminants to the target sample.

2.3. Dwarf/Giant Separation

To separate cool dwarf stars from more-massive, evolved stars with similar $V - J$ color, we used archival trigonometric parallax measurements, when parallaxes were available, and reduced proper motions where parallaxes were not available. For stars with archival parallax observations, we applied the following selection criterion to isolate cool dwarfs, following the approach of Gaidos et al. (2014):

$$M_V > 2.2 \times (V - J) - 2.0. \quad (1)$$

Only 3535 stars in the combined catalog met this criterion. For stars without archival trigonometric parallaxes, we used the reduced proper motion H_V :

$$H_V = V + 5.0 \times \log(\mu) + 5.0 \quad (2)$$

where μ is the proper motion in arcseconds per year. Reduced proper motions have been used by previous authors to identify M dwarfs for exoplanet surveys (e.g., Lépine & Gaidos 2011). Specifically, we adopted the reduced proper motion criteria of Gaidos et al. (2014) for cool dwarfs, except for those with especially red colors. Gaidos et al. (2014) curated a list of bright ($J < 10$) M dwarf stars for the purpose of identifying the best targets for radial velocity surveys. In this work, we extend this approach to the full SUPERBLINK catalog in order to

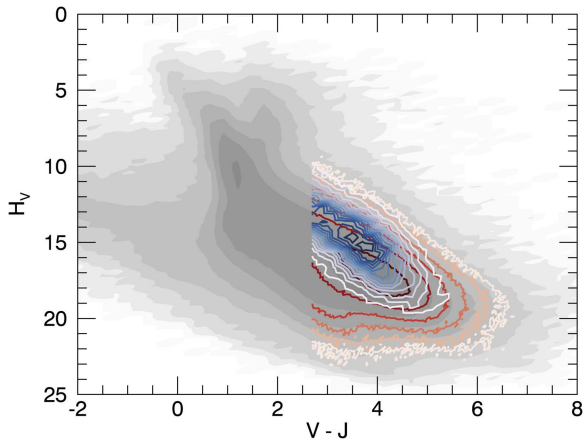


Figure 2. Contours showing the density of stars with reduced proper motion H_V vs. color $V - J$ for all stars in SUPERBLINK (white-to-black color scale), for dwarfs identified by reduced proper motion (white-to-red color scale), and dwarfs identified by trigonometric parallax (white-to-blue color scale). Contours are logarithmically spaced.

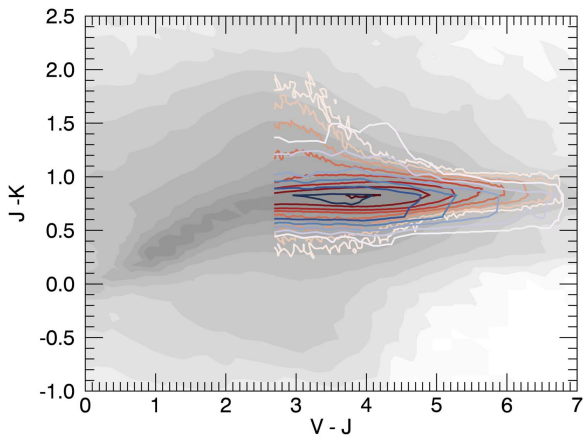


Figure 3. Contours showing the density of stars with colors $J - K$ vs. $V - J$. The color coding is identical to that of Figure 2.

include fainter cool dwarfs, as suited for *TESS*:

$$\begin{aligned} H_V &> 8.806 \\ &+ 2.304 \times (V - J - 2.7) \\ &+ 0.054 \times (V - J - 2.7)^2. \end{aligned} \quad (3)$$

Following the approach of Lépine & Gaidos (2011), we further applied color criteria to help remove evolved stars that may otherwise pass the reduced proper motion criteria. Lépine & Gaidos (2011) initially set relatively stringent color limits in $[J-H, H-K]$ space, but these limits have since been found to exclude very late-type M dwarf stars such as TRAPPIST-1; hence we have modified the boundaries to include such objects. For stars with $H - K < 0.25$, we followed the color criteria of Lépine & Gaidos (2011):

$$J - H < 1.0, \quad (4)$$

$$0.746 < J - K_S < 0.914. \quad (5)$$

However for stars with $H - K \geq 0.25$ we adopted a more liberal limit. This was invoked to increase the numbers of mid-to-late M dwarfs that may have been excluded by the criteria of

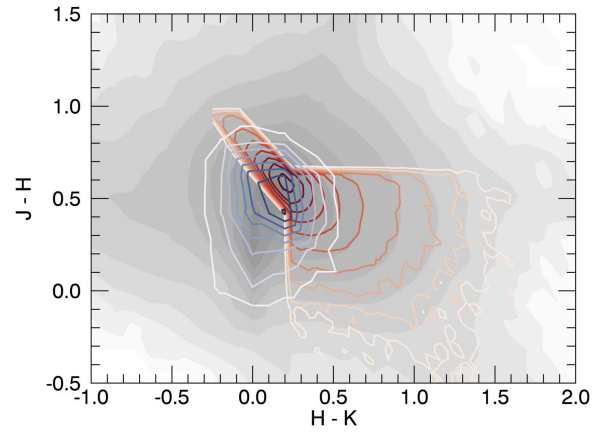


Figure 4. Contours showing the density of stars with colors $J - H$ vs. $H - K$. The color coding is identical to that of Figure 2.

Lépine & Gaidos (2011):

$$J - H < 0.914. \quad (6)$$

Figures 2–4 show all stars in the SUPERBLINK catalog and those identified as cool dwarfs using these criteria, separated into the parallax and proper motion identified stars. Because SUPERBLINK contains stars with high proper motions, giants are largely excluded in the catalog to begin with. After applying these criteria to the combined catalog, we are left with 1076,470 stars that meet the selection criteria, in addition to those with archival trigonometric parallax observations.

SUPERBLINK is known to be less complete for declinations (δ) less than -30° . This is due to the coverage of POSS I and POSS II, which could not observe stars south of $\delta = -30^\circ$ due to the latitude of the 48 inch Samuel Oschin Telescope at Palomar Observatory. Figure 5 shows the resulting catalog of stars across the night sky, in equatorial coordinates.

There are 1039,173 stars in the CDC with $\delta \geq -30^\circ$ and only 40,832 with $\delta < -32^\circ$, owing to the lack of 1950s plate data from POSS-I. However, if only proper motions of greater than 150 mas are considered, the spread of objects is actually uniform across the sky. The significant lack of stars with $\delta < -32^\circ$ presents a challenge to realizing the star counts in S15. Three patches of sky above -32° represent three fields for which 1950s plate data (from POSS-I) is unavailable from the Digitized Sky Surveys.

2.4. Comparison to Galactic Simulations

To explore the completeness of the resulting catalog of cool dwarfs, we can compare the star counts to those predicted by galactic simulations. To simulate the M dwarf counts expected in the night sky, we used the TRIdimensional model of the GALaxy (TRILEGAL, pronounced TREE-leh-GOW; Girardi et al. 2005), and followed an approach nearly identical to that of S15. We used the HEALPix software to determine 3072 equally spaced coordinates across the sky, each centered on a region subtending a solid angle of 13.4 deg^2 (Górski et al. 2005). We neglected coordinates with Galactic latitudes less than 8° due to their proximity to the Galactic plane, where TRILEGAL computations take excessively long. For each coordinate, we queried the TRILEGAL web interface¹⁰ using a

¹⁰ <http://stev.oapd.inaf.it/cgi-bin/trilegal>

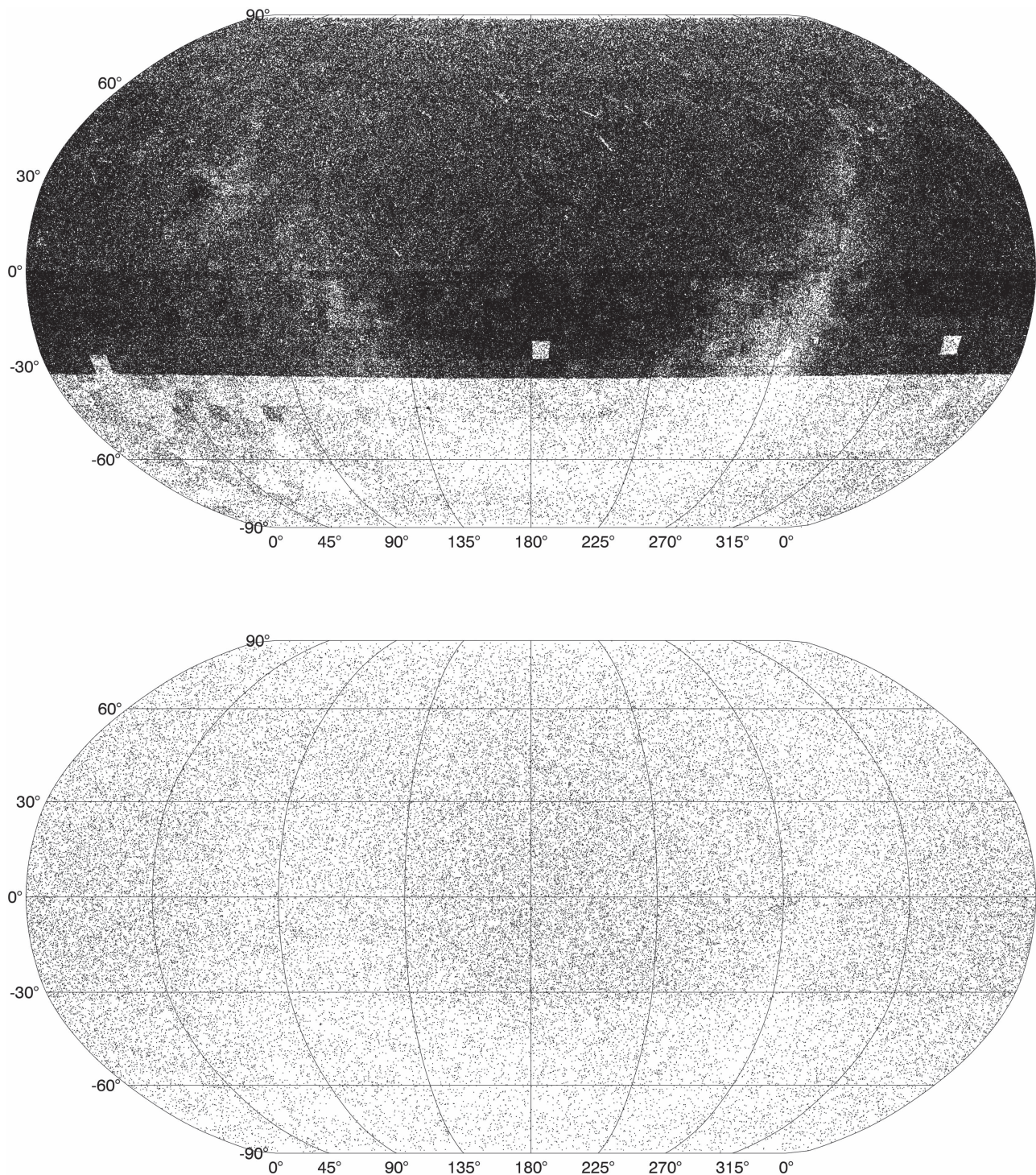


Figure 5. Top: projected sky image of the locations of stars in the Cool Dwarf Catalog (CDC) in equatorial coordinates. The lack of cool dwarfs with $\delta < -32^\circ$ is a consequence of a lack of long-time-baseline proper motion data incorporated into SUPERBLINK. Bottom: same as the top image, but only including stars with proper motions greater than 150 mas, where the catalog is more complete in the south.

Perl script written by L. Girardi and available as part of the VESPA software package (Morton 2012, 2015).

We used the default options in TRILEGAL, but with a solid angle of 6.7 deg^2 , half the 13.4 deg^2 corresponding to each coordinate in order to decrease the computation time. To account for this discrepancy, each star in the resulting simulation was doubled, replicating the approach of S15. We applied a magnitude cut of $V < 20$ as the CDC does not contain stars fainter than this limit. Once downloaded, we applied an absolute

magnitude cut to the simulated stars matching the cut used for cool dwarfs with parallax observations (Equation (1)).

We compared the simulated stars from each TRILEGAL pointing to the detected stars in the CDC, within that same solid angle on the sky. Due to the incompleteness of SUPERBLINK for $\delta < -30^\circ$ we divided the comparison into “north” and “south” groups corresponding to that boundary. Figure 6 shows the resulting completeness of the CDC as a function of V and $V - J$ for stars with $\delta > -30^\circ$ and Figure 7

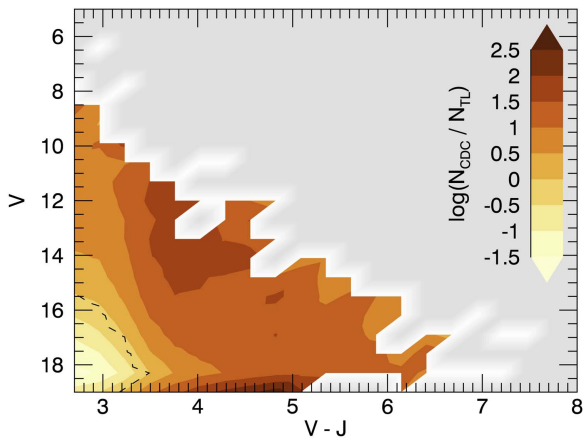


Figure 6. Contour plot showing the log of the number of stars in the CDC divided by the number of stars returned by TRILEGAL, vs. V magnitude and $V - J$ color, for $\delta > -30^\circ$. The contours depict an estimate of the completeness of the catalog compared to models of the galaxy. Grayed areas contain no stars in TRILEGAL, and the dashed contour corresponds to equal numbers of stars in both.

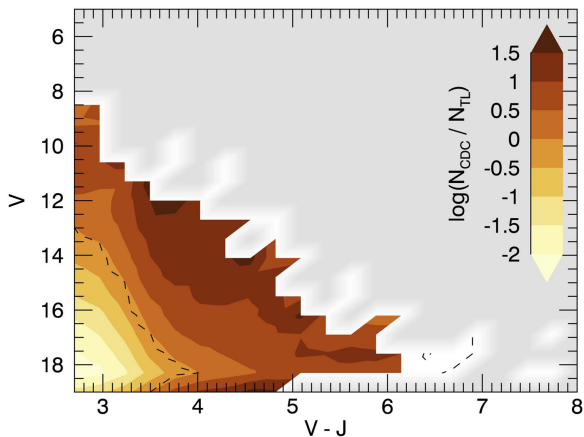


Figure 7. Same as Figure 6, but for $\delta < -30^\circ$.

shows the same for stars with $\delta < -30^\circ$. In both cases, the CDC has more supposed dwarf stars than predicted for most of the phase space, indicating potential contamination by giant stars with erroneous proper motion measurements. This is especially concerning near $V - J \sim 4$ and $V \sim 13$, where the CDC has over 100 times as many objects as predicted by TRILEGAL in the “north” sample. We suspect the inaccuracies of the magnitudes are contributing significantly to the discrepancies in star counts between the catalog and predictions from TRILEGAL.

2.5. Interstellar Extinction and Reddening

Interstellar extinction and reddening can bias the catalog selection, especially for distant stars, where these effects can be especially strong. However, the cool dwarfs considered here are not particularly distant, meaning extinction and reddening may not significantly affect the goals of the catalog. As stated earlier, the optical minus infrared color provides the most leverage when determining an M dwarf temperature. The color chosen in this work, $V - J$, may be affected by reddening. To assess the expected degree of extinction and reddening, we examined the values for extinction in the V -band (A_V) listed in the TRILEGAL simulations. The so-called standard interstellar

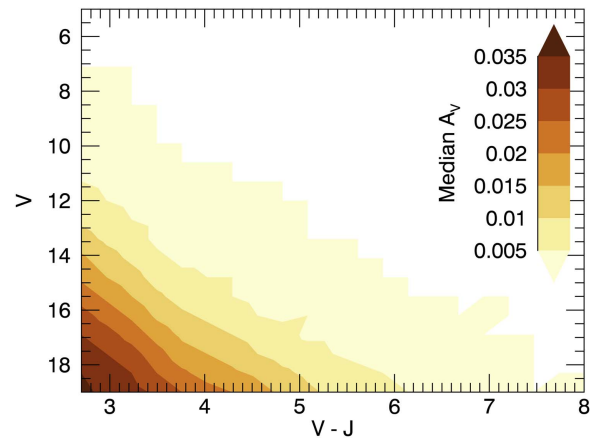


Figure 8. Contour plot showing the median A_V in the TRILEGAL simulations with dwarf criteria applied, vs. V magnitude and $V - J$ color. The maximum extinction is expected to be $A_V = 0.038$, and that primarily applies to the faintest stars and bluest objects in the CDC, which by nature are the most distant.

extinction law measured by Rieke & Lebofsky (1985) calculates A_J/A_V of 0.282 for “standard” lines of sight. Combining these two, we can determine the largest effect expected from interstellar extinction and reddening.

Figure 8 shows the median extinction A_V versus V magnitude and $V - J$ color for the TRILEGAL simulations, subjected to the dwarf selection criteria described previously. As expected, A_V is largest for the faintest and bluest stars, peaking at a value of 0.038. Combining this with A_J/A_V measured by Rieke & Lebofsky (1985), dwarf stars in the CDC are not expected to be reddened by more than $\Delta(V - J) = 0.027$. Given the relatively small size of the effect, we choose to ignore extinction and reddening in our criteria for determining the CDC, as well as for estimating stellar properties, for the sake of reproducibility. We note, however, that any evolved stars that may contaminate the CDC are likely distant and significantly reddened.

2.6. Binarity

Stellar multiplicity of the target sample will have a significant impact on the scientific goals of the *TESS* mission. For widely separated multiple star systems, different apertures can be used to search for transiting planets orbiting each component. However, these objects may not be the best use of limited two minute observations by *TESS*. Recent work by Kraus et al. (2016) showed that stars in multiple systems are less likely to host exoplanets, presumably due to gravitational effects on the individual stars’ protoplanetary disks, or subsequent evolution of planetary orbits.

Unresolved binary or multiple systems present their own challenges. In the case of an unresolved equal mass binary, a given transiting planet will produce a shallower transit depth. This might lead one to abandon any stars that appear to be short-period and unresolved binaries. At the same time, two minute observations of eclipsing binary stars have proven useful for determining highly precise and accurate parameters for the component stars, which are useful for determining the properties of planets found to orbit other single stars. Recently, Shan et al. (2015) calculated the “number of M dwarfs per M dwarf”, in an attempt to determine the short-period binary rate among M dwarf stars using *Kepler* eclipsing binary data. They

found $0.11^{+0.04}_{-0.04}$ of presumably single M dwarfs are actually M dwarfs with a short-period (<90 day) M dwarf companion. However, we note that Fischer & Marcy (1992) found a significantly higher overall M dwarf binary fraction of $42\% \pm 9\%$, but for orbital periods out to 30 yr.

Regardless of whether multiple star systems, resolved or unresolved, should or should not be included in the cool dwarf target list, the fact is that without comprehensive spectroscopy, high-resolution spatial imaging, or trigonometric parallax data, determining multiplicity is prohibitively difficult. The vast majority of stars identified as cool dwarf stars using the approach described above do not have sufficient data to determine whether they host an equal-mass or lower-mass binary star, or multiple stars. For these reasons, we choose to ignore binarity in the determination of this cool dwarf target list. In the proceeding analysis we treat every object in the CDC as a single star. For the vast majority of targets in the CDC, this will have little affect on the errors in the estimated stellar parameters, since the colors are dominated by the primary component. Ironically, this assumption will lead to the largest error in the parameters for stars with trigonometric parallax measurements, whereby the absolute magnitude of a binary is presumed to be due to a single star.

2.7. TESS Magnitudes

In order to choose the best cool dwarfs from the list for two minute observations, we must determine the brightness of the stars within the *TESS* band, or equivalently the *TESS* magnitude T . The *TESS* response function is described in Ricker et al. (2015). Briefly, the response function is optimized for the red end of the visible spectrum, rising sharply redward of 600 nm, then descending gradually from 900 to 1050 nm. As described in S15, in a Vega system T is most similar to Cousins I -band magnitude, or I_C . Unfortunately, I_C is largely unavailable for the vast majority of stars in the catalog. An SDSS-like i' -band is available for many stars via APASS; otherwise, V , J , H , and/or K_s can be used to determine the *TESS* magnitude, as long as effects from spectral type are taken into account.

To assess the role of spectral type when converting magnitude(s) to T , we calculated synthetic photometry from 183 spectro-photometrically calibrated spectra of nearby M dwarf stars. Mann et al. (2015) stitched together visible and near-infrared spectra of nearby M dwarf stars and photometrically calibrated the resulting full spectra. Being stitched across multiple bands and spectrophotometrically calibrated, the spectra are useful for determining conversions between various visible and infrared bands as a function of color or spectral type. The 183 calibrator stars span spectral types from K7 to M7, temperatures from 2700 to 4100 K, masses from 0.08 to $0.74 M_{\odot}$, and iron abundances ($[Fe/H]$) from -0.61 to 0.53.

For each of the spectro-photometrically calibrated spectra, we multiplied by the response functions for i' , T and for 2MASS J , H , and K_s . For each case, we calculated the resulting colors and fitted three magnitude conversion equations: one using i' and K_s magnitude, one using V and K_s , and one using J , H , and K_s :

$$T = 0.6262 + 1.0004 \times i' - 0.3326 \times (i' - K_s) \quad (7)$$

$$T = 0.8536 + 0.9972 \times V - 0.6793 \times (V - K_s) \quad (8)$$

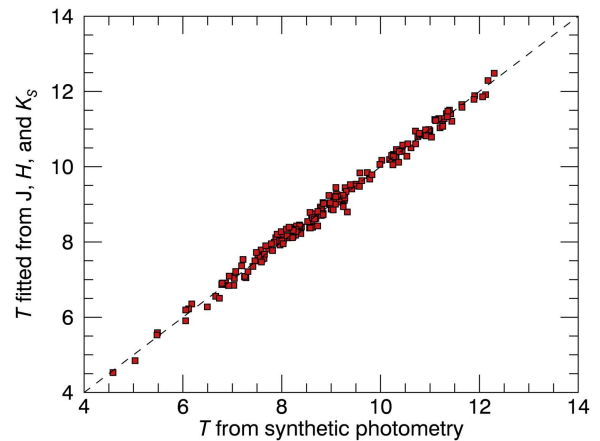


Figure 9. Synthetic *TESS* magnitude (T) vs. T derived from the conversion from 2MASS magnitudes (see Equation (9)) for spectro-photometrically calibrated spectra from Mann et al. (2015). The root mean square of the residuals is 0.14 mag.

$$T = 0.6316 + 1.0329 \times J - 0.4324 \times (J - H) + 4.0239 \times (H - K_s). \quad (9)$$

The root mean square residuals for each of the fitted relations are 0.030, 0.055, and 0.14 mag, respectively. The final relation has the largest scatter because it uses infrared magnitudes to determine a visible magnitude. However, for many of the stars in the CDC, only 2MASS magnitudes are uniformly measured.

Figure 9 plots T calculated via synthetic photometry versus T determined using Equation (9), for the calibration spectra. To determine T for each star in the CDC, we use Equation (7) if either APASS or SDSS i' is available. However, we found that for the calibration sample, the SDSS synthetic magnitudes did not match measured APASS magnitudes of the stars. We applied a conversion from APASS i' to SDSS i' prior to using Equation (7) based on this discrepancy.

If i' is not available, we use Equations (8) and (9) and take the weighted mean between the two, weighting by their respective uncertainties. For those uncertainties, we propagate the reported or assigned V , i' , J , H , and K_s uncertainties through the equations and, in the case of Equation (9), we add a systematic uncertainty of 0.14 mag in quadrature to account for the systematic error in the fitted conversion.

2.8. Effective Temperatures

We determine an effective temperature (T_{eff}) for each cool dwarf in the catalog using the color- T_{eff} relations from Mann et al. (2015, 2016). Specifically, we use the $r - J$, $r - z$, and/or $V - J$ relations, depending on available magnitudes, and we include a $J - H$ term to account for systematic effects of metallicity on the resulting effective temperature (see Johnson et al. 2012; Mann et al. 2013a; Newton et al. 2014). Because of the requirements for target selection (Section 2.2), all targets have at least one of these colors, with all having at least a V and J magnitude. For targets with more than one color available we use the weighted mean of the derived T_{eff} as the final value. We note that very few targets have reliable z -band observations, and that particular relation is rarely invoked.

For stars with APASS r' magnitudes, we again apply a correction to convert to SDSS r' magnitudes, based on the

discrepancy between measured APASS r' and synthetic SDSS r' magnitudes on the spectro-photometric calibration sample.

Errors on T_{eff} are computed by combining errors due to magnitude uncertainties, scatter in the color– T_{eff} relations, and the intrinsic scatter in the Mann et al. (2015) calibration sample (60 K). The calibration sample of Mann et al. (2015) contains no stars with $V - J > 7$ ($r - J \lesssim 6.2$, $T_{\text{eff}} \lesssim 2700$). For stars beyond this limit we do not assign a T_{eff} , but we keep those stars in the catalog for completeness.

2.9. Masses and Radii

For cool dwarfs with trigonometric parallaxes, we first calculate the absolute K_s magnitude and associated error from its 2MASS magnitude. We convert M_{K_s} to mass using the $M_{K_s} - M_*$ relation from Benedict et al. (2016), a fifth-degree polynomial. This relation is calculated using dynamical masses of low-mass binary stars, and is valid for $5.2 < M_{K_s} < 11$. To calculate the uncertainty in mass, we propagate the uncertainty M_{K_s} through the polynomial, as well as the uncertainties in the polynomial coefficients themselves. The coefficients have non-zero covariances, and we include the reported covariances when determining the uncertainty.

For cool dwarfs with $4.5 < M_{K_s} < 5.2$ we use the Delfosse et al. (2000) $M_{K_s} - M_*$ relation, which is similarly calibrated on dynamical masses, but has fewer calibration stars than Benedict et al. (2016). However, the latter work's relations are not valid over this regime whereas the former's are. We follow an uncertainty procedure nearly identical to what is describe above, but do not propagate the uncertainties in the coefficients themselves, as these are not reported in Delfosse et al. (2000).

We then calculate stellar radii using the $M_{K_s} - R_*$ relation from Mann et al. (2015), which is precise to $\simeq 3\%$ ignoring errors in K_s and distance. We calculate uncertainties in stellar radius by propagating the uncertainty in M_{K_s} through the relationship, then incorporate a 3% systematic uncertainty by adding the uncertainty in quadrature.

For stars lacking a trigonometric parallax, or the vast majority of the catalog, we determine radius using the $T_{\text{eff}} - R_*$ relation from Mann et al. (2015). For masses we derive a new relation between T_{eff} and M_* based on the 183 M dwarfs with precise distances and radii collected by Mann et al. (2015), but deriving new masses for these stars based on the Benedict et al. (2016) $M_{K_s} - M_*$ relation to keep the masses consistent with our parallax-based values.

Radii and masses derived from T_{eff} are almost always less precise than those derived using M_{K_s} , with best case errors on radius of $\simeq 3\%$ in the latter case, and 13% in the former. This is primarily due to the important role metallicity plays in the relation between luminosity and T_{eff} for M dwarfs, of which M_K is relatively immune (Delfosse et al. 2000; Mann et al. 2015), and the steep relation between T_{eff} and R_* compared to between M_{K_s} and R_* for M dwarfs.

2.10. The Cool Dwarf Catalog

The final catalog contains 1080,005 entries. Table 1 shows the column headings for the catalog and a link to the full catalog in the supplementary data of this paper. We report identifiers, the J2000 equatorial coordinates, the chosen V magnitude, the calculated *TESS* magnitude T , T_{eff} , radius, mass, corresponding uncertainties, and flags. For each entry, we also include the columns available from SUPERBLINK, 2MASS,

Table 1
Column Headings for the Cool Dwarf Catalog

Column Heading	Description
TMCNTR	Parameter used for cross-matching catalogs
SBLINK	Superblink star designation
RA	R.A. in decimal degrees (J2000)
DEC	Decl. in decimal degrees (J2000)
VMAG	V magnitude
e_VMAG	Uncertainty in VMAG
f_VMAG	Flag indicating source for VMAG
TESS MAG	<i>TESS</i> Magnitude
e_TESS MAG	Uncertainty in <i>TESS</i> MAG
f_TESS MAG	Flag indicating method for determining <i>TESS</i> MAG
TEFF	Effective temperature
e_TEFF	Uncertainty in TEFF
f_TEFF	Flag indicating method for determining TEFF
RADIUS	Stellar radius
e_RADIUS	Uncertainty in RADIUS
f_RADIUS	Flag indicating method for determining RADIUS
MASS	Stellar mass
e_MASS	Uncertainty in MASS
f_MASS	Flag indicating method for determining MASS
SBLINK	SUPERBLINK columns
APASS	APASS columns
2MASSID	2MASS Source designation
GAIA SOURCEID	<i>Gaia</i> Source ID

(This table is available in its entirety in machine-readable form.)

and APASS verbatim for completeness. If a particular parameter could not be computed, or is not present in a catalog, the specific entry is left blank.

The J2000 coordinates are taken from SUPERBLINK, which sets all the coordinates to the 2000.0 epoch, extrapolating from the 2MASS coordinates/epochs using the measured proper motion vectors. The flag assigned to the V magnitude can take one of three strings: *apass*, *tycho*, or *sblink*, indicating the source of the chosen V magnitude. The flag assigned to the *TESS* magnitude T can take one of five flags: *from_apass_ik*, *from_sdss_ik*, *wmean_vk_jhk*, *vk*, or *no_kmag*. The first two use a combination of i band (from either APASS or SDSS, respectively) and 2MASS K band to determine T . The third uses a weighted mean between the $V - K$ relation and the 2MASS only relation. The fourth uses only $V - K$, and the fifth indicates that the object does not have a reliable K -band magnitude, so a *TESS* magnitude could not be reliably determined.

The T_{eff} flag is a combination of letters indicating which colors were used to determine the effective temperature. The combination can include *rj*, *vj*, and/or *rz*, each corresponding to the color used. The final T_{eff} is the weighted average of all the color– T_{eff} relations used. The radius flag can take one of three strings: *from_teff*, indicating that it was determined from T_{eff} , *from_mk*, indicating it was determined from the absolute K -band magnitude (Mann et al. 2015), or *no_radius*, indicating that it could not be determined. Similarly, the mass flag can take one of several strings:

from_teff, from_mk_D00, indicating the Delfosse et al. (2000) relations were used, from_mk_B16, indicating the Benedict et al. (2016) relations were used, or no_mass, indicating it could not be determined.

2.11. Incorporation into the TIC and CTL

The CDC is currently incorporated into the TIC and *TESS* CTL, both of which are described in Stassun et al. (2017). Briefly, the TIC is an omnibus catalog with the goal of listing all stars that fall within the field of view and brightness limit of *TESS* during the primary mission, similar in scope to the *Kepler* Input Catalog for the *Kepler* mission (Batalha et al. 2010; Brown et al. 2011). The CTL is a subset of the TIC containing stars that will be observed using two minute cadence, specifically for searching for transiting exoplanets.

The TIC master database stores the CDC in its own table. The catalog is matched against the rest of the TIC entries. In the event that stars in the CDC already exist in the TIC, the latter retains both parameters (those already in the TIC and those in the CDC); however, when choosing stars for the CTL, the process uses the parameters in the CDC, as determined by the methods described in this paper. When revised versions of the CDC have been uploaded to the TIC, the latter retains the superseded versions of the CDC, but the CTL does not. When revised versions of the CDC are submitted, stars deleted from the prior version are deleted from the CTL.

For *TESS*, the CDC serves as an “overriding, curated catalog.” Stellar parameters such as *TESS* magnitude, radius, effective temperature, and derived values already in the TIC are overwritten by values reported in the CDC. There are a few cases, however, where effective temperature and/or radius have not been reported in the CDC. In these cases the values already in the TIC are retained.

2.12. Comparisons between Parallax and Magnitude Determinations

To test the accuracy of the stellar parameters as determined from magnitudes alone, we use those cool stars with parallax observations. Figure 10 shows the masses and radii as determined from trigonometric parallaxes, compared to those determined using magnitudes via the estimated effective temperature. The root mean square deviation between the magnitude and parallax determinations is $0.145 M_{\odot}$ and $0.120 R_{\odot}$ for the mass and radius determinations, respectively. The root median square deviation, a statistic less sensitive to outliers, between the magnitude and parallax determinations is $0.097 M_{\odot}$ and $0.081 R_{\odot}$ for the mass and radius determinations, respectively.

It is clear from Figure 10 that the mass and radius estimates from photometry alone have systematic errors, especially between 0.2 and $0.3 M_{\odot}$ and R_{\odot} , where the photometric relations appear to over-predict them. Such systematic errors are prevalent when using photometry alone to estimate stellar parameters of low-mass stars. We note that the *Kepler* Input Catalog also faced systematic uncertainties in cool dwarf parameters, described by Brown et al. (2011) and measured via spectroscopy by Muirhead et al. (2012, 2014). Recently, Dressing et al. (2017a, 2017b), Martinez et al. (2017), and Hirano et al. (2018) acquired spectra for cool dwarf planet hosts from NASA’s *K2* mission, again revising stellar and planetary parameters originally determined by photometry. We

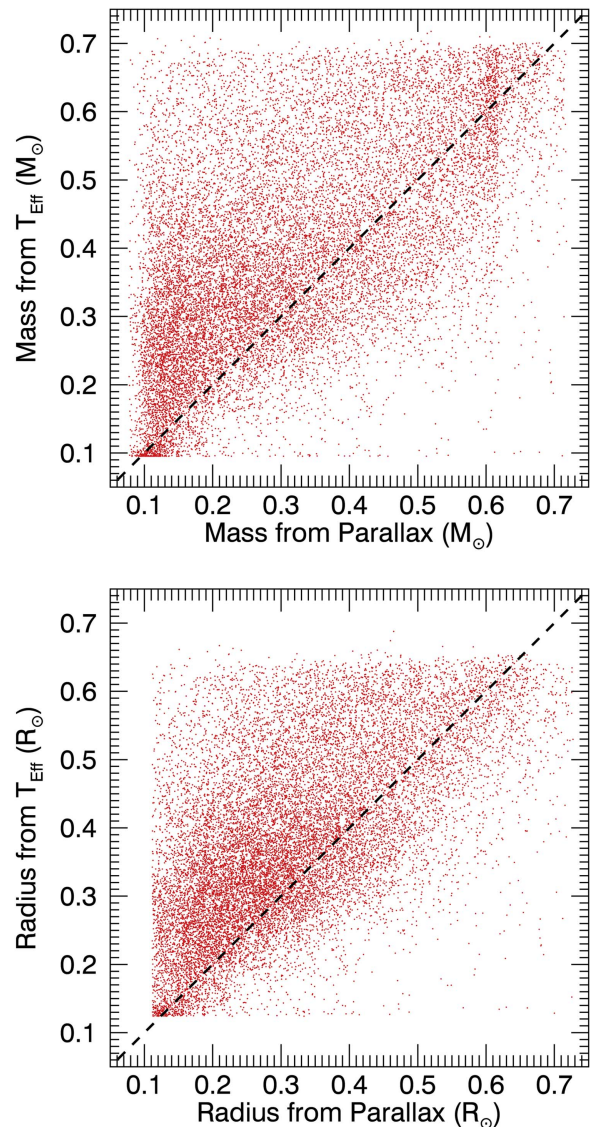


Figure 10. Top: stellar mass determined from parallaxes vs. stellar mass determined from T_{eff} , for stars in the catalog with astrometric parallaxes from the literature. Bottom: the same, but for stellar radius.

fully expect to revise the masses and radii of the objects in the CDC as astrometric parallaxes become available from the *Gaia* mission, as well as add additional objects primarily in the southern ecliptic hemisphere.

2.13. Caveats and Warnings

While the simplicity of the above methods for deriving properties of M dwarfs makes it easier to reproduce, and hence useful for the large catalog of stars required, there are a number of important caveats that one should consider when using these parameters.

1. All targets are assumed to be late K or M dwarfs. Reddened K stars, stars with inaccurate colors, or evolved stars with large or erroneous proper motions in the final sample, will have faulty assigned stellar parameters.
2. Radii and masses derived from M_K , will be systematically large if the target is an unresolved binary. For

near-equal-mass binaries, this effect can result in derived radii as much as 30% larger than the true value, significantly larger than the typical errors. Some of these systems could be identified by their position on a color–magnitude diagram (CMD). In practice, however, binaries are difficult to disentangle from metal-rich stars, due to the strong effect of metallicity on CMD position for M dwarfs (Johnson & Apps 2009; Schlaufman & Laughlin 2010; Neves et al. 2012), and employing such a correction might bias the sample in unintended ways.

3. Because metallicities are not known, masses and radii derived using T_{eff} will be systematically too large for metal-poor stars and systematically too small for those that are metal-rich. A small correction for this could be to include $J - H$ colors as a proxy for $[\text{Fe}/\text{H}]$ in the $T_{\text{eff}}-R_*$ calculation, as was done when converting colors to T_{eff} . However, a color-based metallicity correction to the radius– T_{eff} relation has not been empirically calibrated to date. Therefore, we chose not to apply this correction.
4. For parallax- or T_{eff} -based methods, relations from Mann et al. (2015) are only valid over $-0.6 < [\text{Fe}/\text{H}] < 0.4$, and the Benedict et al. (2016) calibration sample is mostly near solar metallicity. For stars well below this range or with unusual abundance patterns (e.g., high C/O) the relations may be completely invalid.
5. There are significant systematic differences between different sources of photometry due to color terms (Bessell & Murphy 2012; Mann & von Braun 2015). These terms are largest for the reddest stars, so this may be significant for M dwarfs in our sample.
6. We assumed all stars are on the main sequence. Extremely young stars ($\lesssim 30$ Myr) are likely a small fraction of our sample, and would be best handled using completely different techniques. Similarly, we assume stars are not being inflated by activity, whether through youth or external factors (e.g., a tight binary). The size of this effect is debated (e.g., Kraus et al. 2011; Stassun et al. 2012; Mann et al. 2015, 2017), and we have no activity measurements across the majority of the sample, making it difficult to apply a correction.

3. Planet Yields

We estimated the anticipated planet yield from *TESS* observations of cool dwarfs by assigning planets to the stars using the occurrence rates derived from analyses of *Kepler* data and determining the number of planets that could be detected by *TESS*. We began by constructing a fine grid in planet radius and orbital period space using the same boundaries as in Figure 11 of Dressing & Charbonneau (2015).

Next, we determined the transit depths and durations for planets at the centers of each grid cell in orbit around the stars in the cool dwarf sample. We restricted our analysis to the 1140,164 stars with assigned temperatures and masses in the range $0.08 M_{\odot} - 0.73 M_{\odot}$. For each star/planet combination, we predicted the signal-to-noise ratio (S/N) for a single transit by comparing the expected transit depth to the noise predicted by the relations in S15. Our noise estimates incorporated shot noise, sky noise, readout noise, stellar noise, and a 60 ppm noise floor due to systematic effects, a conservative estimate. Following S15, we included stellar noise by randomly assigning each star a noise level matching that of one of the

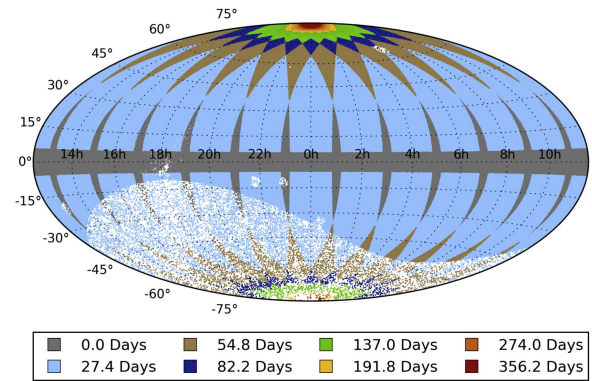


Figure 11. Map (in ecliptic coordinates) showing the number of days of data that could be obtained for each star in the CDC. Note that we assumed an arbitrary ecliptic longitude for the center of the first field.

99 moderately bright ($12.5 < m_{\text{Kep}} < 13.1$) *Kepler* cool dwarfs studied by Basri et al. (2013). The distribution of assigned variabilities extended from 26 ppm to 1% with a mean value of 326 ppm. Our noise estimates did not consider flux contamination due to nearby stars.

After estimating the single transit S/N (S/N_{single}), we calculated the cumulative multiple transit S/N (S/N_{multi}) by first determining the number of days that *TESS* could observe each star and then scaling S/N_{single} by the square root of the total number of transits. We estimated survey coverage by using a modified version of the *tvguide* tool developed by the *TESS* GI office (Mukai & Barclay 2018) assuming an arbitrary initial ecliptic longitude for the center of the first field (see Figure 11). We considered planets to be “detected” if S/N_{multi} exceeded 7.1σ , even if only one transit occurred within the observing window.

We accounted for the geometric consideration that not all planets will appear to transit. For each star, we generated a map of the occurrence rate of transiting planets by multiplying the occurrence rates from Dressing & Charbonneau (2015) by the geometric likelihood of transit R_*/a at the center of each grid cell. We then computed the number of detected planets per star by summing the occurrence rates of transiting planets in detectable grid cells (i.e., grid cells for which the $S/N_{\text{multi}} > 7.1\sigma$).

Finally, we estimated the total planet yield from the full cool dwarf population by adding the contributions from each star. In total, we anticipated that *TESS* would detect 2136 planets with radii $0.5 R_{\oplus} < R_p < 4 R_{\oplus}$ and periods $0.5 < P < 200$ day if all stars in the CDC were monitored at two minute cadence when they were visible to *TESS*, assuming all objects were indeed M dwarfs. Subdividing the planets by radius, we anticipated that *TESS* would detect roughly 151 Earth-sized planets ($R_p < 1.25 R_{\oplus}$), 504 super-Earths ($1.25 R_{\oplus} < R_p < 2 R_{\oplus}$), and 1481 sub-Neptunes ($2 R_{\oplus} < R_p < 4 R_{\oplus}$) orbiting cool dwarfs. The typical *TESS* cool dwarf planet would be a $2.3 R_{\oplus}$ planet with a 7 day orbital period. However, we note that only 200,000 to 400,000 stars will be monitored in two minute cadence and that not all two minute targets will be cool dwarfs. We discuss the selection of best objects for two minute cadence in Section 3.1.

3.1. Prioritizing Targets for Two Minute Cadence

The cool dwarf target list contains over 1 million stars, which is ten times larger than the set of stars that will be observed at two minute cadence. In order to investigate which

cool dwarfs would benefit most from two minute cadence, we begin by considering the dependence of the transit duration on host star properties. Following Winn (2010) and making the simplifying assumptions that (1) the planet is much smaller than the star, (2) the planet follows a circular orbit, (3) the orbital semimajor axis a is much larger than the stellar radius R_* , and (4) the planet transits directly across the center of the star, the approximate transit duration is

$$T \approx \frac{R_* P}{\pi a} \quad (10)$$

where P is the planetary orbital period. Using *Kepler's* third law to rewrite a in terms of P and combining the stellar mass and radius terms into stellar density ρ_* , the expression becomes

$$T \approx 13 \text{ hr} \left(\frac{P}{1 \text{ year}} \right)^{1/3} \left(\frac{\rho_*}{\rho_\odot} \right)^{-1/3}. \quad (11)$$

If we then enforce the (arbitrary) requirement that *TESS* obtain at least n data points during each transit event, then we find that two minute cadence observations are required for stars with densities

$$\frac{\rho_{*,\text{threshold}}}{\rho_\odot} \gtrsim \left(\frac{1}{n} \frac{13 \text{ hr}}{0.5 \text{ hr}} \right)^3 \left(\frac{P}{1 \text{ year}} \right) = \frac{48}{n^3} \left(\frac{P}{1 \text{ day}} \right). \quad (12)$$

For a fiducial orbital period of 0.5 day, the critical stellar density required to obtain one point per transit is $\rho_{*,\text{threshold}} = 24\rho_\odot = 34 \text{ g cm}^{-3}$, which roughly corresponds to stellar masses $\lesssim 0.15 M_\odot$. If we instead change the fiducial orbital period to two days and require two points per transit, the critical stellar density decreases to 17 g cm^{-3} , increasing the stellar mass cutoff to $\lesssim 0.27 M_\odot$. Clearly, the choice between two minute and 30 minute cadence is strongly dependent on the targeted orbital period range. Maximizing the yield of ultra-short period planets would require that the majority of cool dwarfs be observed at two minute cadence.

Given the practical limitations on the number of cool dwarfs that can actually be monitored at two minute cadence, one strategy for selecting two minute cadence targets would be to prioritize cool dwarfs that are bright enough for follow-up observations. While there are 326,039 cool dwarfs with densities higher than 17 g cm^{-3} , only 5243 have $T < 13$. A fraction of these stars are likely to be unobservable due to gaps between detectors and proximity to extremely bright stars, further reducing the required number of two minute cadence pixels.

3.2. Considering Characterization

Even if two minute cadence is not required to detect planets orbiting larger cool dwarfs or planets with longer orbital periods, acquiring observations at shorter cadence significantly improves the precision of stellar parameter estimates. For instance, the impact parameter can be constrained much more precisely when the shape of the transit profile is captured. In turn, narrowing the allowed range of impact parameter improves the constraints on planet radius.

Transit durations are also much easier to measure with high-cadence photometry. Accordingly, estimating the orbital periods of single-transit events will be less challenging if those transits happen to be observed at two minute cadence. Due to their longer orbital periods, singly transiting planets are likely

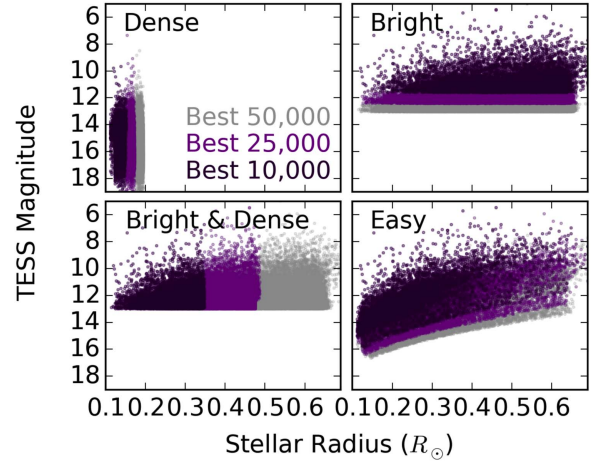


Figure 12. Comparison of the brightnesses and radii of stars selected for observation at two minute cadence using various prioritization schemes, listed in each quadrant. Within each panel, the best 10,000 stars are shown in dark purple, stars within the best 25,000 are shown in purple, and stars within the best 50,000 are shown in gray.

to be some of the most enticing targets from a planetary habitability perspective, so having the ability to determine their ephemerides and recover their transit windows would be advantageous. Such systems are significantly more compelling if they orbit stars bright enough for atmospheric studies or planetary mass measurement, presenting another justification for prioritizing the cool dwarf target list by host star magnitude and follow-up potential as well as planet detectability.

The final choices of how many cool dwarfs should be observed at two minute cadence and how those targets should be selected are beyond the scope of this paper and will be decided by the *TESS* mission and Guest Investigator Office. In order to help inform that decision, we now study how four extreme choices of prioritization schemes might influence the yield of small planets orbiting cool dwarfs. For each simulation, we select the best 25,000 stars according to the following criteria.

1. *Dense Stars*. As shown in Equation (11), planets orbiting denser stars have shorter transit durations. This prioritization scheme aims to maximize the yield of (ultra-) short-period planets by preferentially reserving two minute cadence observations for the densest cool dwarfs.
2. *Bright & Dense Stars*. Selecting targets by density alone strongly biases the sample toward faint late M dwarfs that are challenging targets for planet detection and follow-up observations due to low photon counts. This scheme uses the same density ranking as the “Dense Stars” scheme but requires that all stars have $T < 13$.
3. *Bright Stars*. If the goal of detecting planets with *TESS* is to identify a sample of planets amenable to follow-up mass measurement and atmospheric characterization, then bright host stars are advantageous. This scheme ranks targets by *TESS* magnitude.
4. “*Easy Stars*”. Selecting easier search targets is attractive because search incompleteness is lower and a higher planet yield could be detected using a smaller target list. This prioritization scheme orders targets by the cumulative S/N expected due to multiple transits of an Earth-radius planet with a period of 7 days.

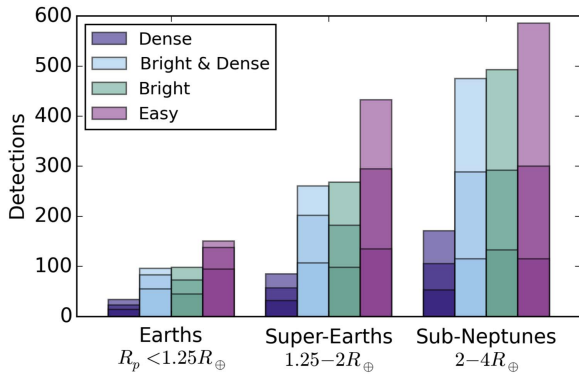


Figure 13. Number of expected detections as a function of planet radius for four notional target prioritization schemes. For each scheme, the short, medium, and tall bars indicate the number of planets that would be detected if the best 10,000, 25,000, or 50,000 stars were selected according to the chosen prioritization scheme.

Overall, the *TESS* mission is expected to monitor 200,000–400,000 stars at two minute cadence, so selecting 25,000 stars is akin to devoting 6%–13% of the observing time to cool dwarfs. In addition to these baseline simulations, we also run “bottom-heavy” and “top-heavy” simulations in which we select 50,000 and 10,000 cool dwarfs per mission. We display the stars selected for each simulation in Figure 12. As expected, the “Dense” and “Bright” samples contain small stars and bright stars, respectively. The “Bright & Dense” sample spans approximately the same magnitude range as the “Bright” sample, but is biased toward smaller stars. The “Easy” sample contains a mixture of smaller, fainter stars and larger, brighter stars.

Comparing the resulting planet yields, we found that the choice of prioritization scheme has a dramatic effect on the number of detected planets. We display the resulting size distributions of detected planets for all four prioritization schemes in Figure 13. In general, the “Dense” scheme recovers far fewer planets than all other proposed schemes: observing the 10,000 densest stars would yield detections of only 14 Earth-sized planets ($R_p < 1.25 R_\oplus$), 32 super-Earths ($1.25\text{--}2 R_\oplus$), and 53 Sub-Neptunes ($2\text{--}4 R_\oplus$). For comparison, observing the 10,000 brightest stars or the 10,000 “easiest” stars would yield roughly 45 Earths, 98 super-Earths, and 133 sub-Neptunes or 95 Earths, 135 super-Earths, and 115 sub-Neptunes, respectively. Considering that the “Easy” scheme selects targets based on small planet detectability, the result that this scheme finds the highest number of Earths is not surprising. The “Bright” survey performs better than the “Easy” survey in terms of the number of sub-Neptune detections (133 planets versus 115 if 10,000 stars are observed), but the latter survey detects a larger population of smaller planets.

The relatively poor yield from the “Dense” scheme is likely due to the faintness of the densest stars. Although short-period planets orbiting those stars would transit very quickly, there is little benefit to observing them at two minute cadence if the photon counts are too low to permit planet detection. We therefore recommend against using stellar density alone to select two minute cadence targets. However, stellar density may be a useful selection criterion when used in combination with other metrics. For instance, we find that a survey of the 10,000 best “Bright & Dense” stars would detect 55 Earths, 107 Super-Earths, and 115 Sub-Neptunes.

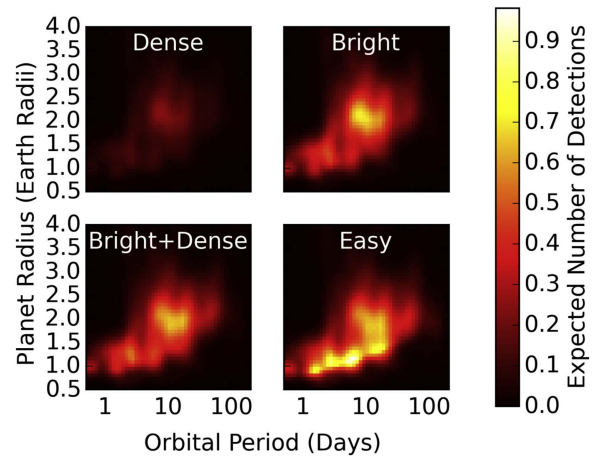


Figure 14. Number of expected detections as a function of planet radius and orbital period for four notional target prioritization schemes. For each scheme, the color indicates the expected number of detections per grid cell. We selected 10,000 target stars per simulation.

The differences in the populations of detected planets are highlighted in Figure 14, which shows heatmaps of the detected planet yield as a function of planet radius and orbital period. The trace for the “Dense” survey is barely noticeable, demonstrating that the stars with the highest densities are challenging transit targets. The heatmap for the “Bright” survey displays a clear pileup of planets with periods near 10 days and sizes of roughly $2 R_\oplus$. These planets would be viable targets for atmospheric characterization and possibly mass measurement. The same planet pileup is noticeable in the “Bright & Dense” heatmap, but the overall distribution of planets is flatter. Unlike the other distributions, the heatmap for the “Easy” survey displays an enticing ridge of planet detections at small radii ($0.8\text{--}1.5 R_\oplus$) and short orbital periods (1.5–20 days). Detecting planets like these would be an excellent opportunity to determine the prevalence and composition of smaller planets.

4. Discussion

We have presented an all-sky catalog of cool dwarf targets for the TIC based largely on archival photometry, parallaxes (where available), and reduced proper motions. We estimated the stellar properties of the cool dwarfs in the catalog based on archival relationships between color, temperature, stellar mass, and stellar radius. We also estimated each star’s *TESS* magnitude (T), for the purpose of estimating the ability to detect transiting planets around each star.

We purposefully ignored the role of binarity and interstellar reddening on the properties listed in the catalog. We ignored binarity because it is difficult to determine the binarity of the stars in the sample with the archival data and it is unclear how this should affect the choice of exoplanet search targets. We ignored reddening as it was calculated to have a marginal affect on the reported stellar properties.

Lastly, we considered several prioritization schemes to determine which of the stars in the CDC would benefit significantly from two minute observations. We used results from NASA’s *Kepler* mission to estimate the planet population around the stars in the CDC. We found that prioritizing the targets based on stellar density would result in far fewer planet detections than prioritizing based on signal-to-noise or star brightness. We found that prioritizing stars based on signal-to-noise (“Easy”)

or star brightness (“Bright”) results in a similar number of detections, but that the “Easy” yield would contain more small planets. Our yield simulations did not consider the effects of flux contamination due to nearby stars or the coplanarity of multi-planet systems. See Ballard (2018) for a detailed analysis of how the low mutual inclinations of planets in multi-planet systems could increase the planet yield.

With the anticipated release of parallax observations from the *Gaia* mission, many of the stellar properties in this catalog will be revised. Until then, however, it serves as a catalog of cool dwarf targets for the *TESS* Mission, including the primary science mission and Guest Observer programs. The CDC has been incorporated into the TIC and is available machine readable format in Table 1.


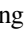




We would like to thank George Ricker, Keivan Stassun, Joshua Pepper, and the entire *TESS* Star Properties Working Group for encouraging this work in support of the *TESS* mission. We would like to thank Michael Cushing for pointing out the importance of coefficient covariances in mass–luminosity relations. We would like to thank Josh Winn and Luke Bouma for sharing their insight on planet yields.

P.S.M. acknowledges support from the NASA Exoplanet Research Program (XRP) under Grant No. NNX15AG08G issued through the Science Mission Directorate. B.R.-A. acknowledges the support from CONICYT PAI/Concurso Nacional Inserción en la Academia, Convocatoria 2015 79150050. This work was performed in part under contract with the Jet Propulsion Laboratory (JPL) funded by NASA through the Sagan Fellowship Program executed by the NASA Exoplanet Science Institute. This research has made use of the NASA Exoplanet Archive, which is operated by the California Institute of Technology, under contract with the National Aeronautics and Space Administration under the Exoplanet Exploration Program (Akeson et al. 2013).

This work has made use of data from the European Space Agency (ESA) mission *Gaia* (<https://www.cosmos.esa.int/gaia>), processed by the *Gaia* Data Processing and Analysis Consortium (DPAC, <https://www.cosmos.esa.int/web/gaia/dpac/consortium>). Funding for the DPAC has been provided by national institutions, in particular the institutions participating in the *Gaia* Multilateral Agreement.

Software: HEALPix (Górski et al. 2005), TRILEGAL (Girardi et al. 2005), VESPA (Morton 2012, 2015).

ORCID iDs

Philip S. Muirhead  <https://orcid.org/0000-0002-0638-8822>
 Courtney D. Dressing  <https://orcid.org/0000-0001-8189-0233>
 Andrew W. Mann  <https://orcid.org/0000-0003-3654-1602>
 Bárbara Rojas-Ayala  <https://orcid.org/0000-0002-0149-1302>
 Sébastien Lépine  <https://orcid.org/0000-0002-2437-2947>
 Martin Paegert  <https://orcid.org/0000-0001-8120-7457>
 Nathan De Lee  <https://orcid.org/0000-0002-3657-0705>
 Ryan Oelkers  <https://orcid.org/0000-0002-0582-1751>

References

Akeson, R. L., Chen, X., Ciardi, D., et al. 2013, *PASP*, 125, 989
 Ballard, S. 2018, arXiv:1801.04949
 Basri, G., Walkowicz, L. M., & Reiners, A. 2013, *ApJ*, 769, 37
 Batalha, N. M., Borucki, W. J., Koch, D. G., et al. 2010, *ApJL*, 713, L109
 Belu, A. R., Selsis, F., Morales, J.-C., et al. 2011, *A&A*, 525, A83
 Benedict, G. F., Henry, T. J., Franz, O. G., et al. 2016, *AJ*, 152, 141

Berta, Z. K., Irwin, J., & Charbonneau, D. 2013, *ApJ*, 775, 91
 Bessell, M., & Murphy, S. 2012, *PASP*, 124, 140
 Bessell, M. S., & Brett, J. M. 1988, *PASP*, 100, 1134
 Boyajian, T. S., von Braun, K., van Belle, G., et al. 2012, *ApJ*, 757, 112
 Brown, T. M., Latham, D. W., Everett, M. E., & Esquerdo, G. A. 2011, *AJ*, 142, 112
 Crossfield, I. J. M., Ciardi, D. R., Petigura, E. A., et al. 2016, *ApJS*, 226, 7
 Cutri, R. M., Skrutskie, M. F., van Dyk, S., et al. 2003, *yCat*, 2246, 0
 Delfosse, X., Forveille, T., Ségransan, D., et al. 2000, *A&A*, 364, 217
 Deshpande, R., Blake, C. H., Bender, C. F., et al. 2013, *AJ*, 146, 156
 Djorgovski, S. G., Gal, R. R., de Carvalho, R. R., et al. 2002, *BASS*, 34, 743
 Dressing, C. D., & Charbonneau, D. 2013, *ApJ*, 767, 95
 Dressing, C. D., & Charbonneau, D. 2015, *ApJ*, 807, 45
 Dressing, C. D., Newton, E. R., Schlieder, J. E., et al. 2017a, *ApJ*, 836, 167
 Dressing, C. D., Vanderburg, A., Schlieder, J. E., et al. 2017b, *AJ*, 154, 207
 Fischer, D. A., & Marcy, G. W. 1992, *ApJ*, 396, 178
 Gaia Collaboration, Brown, A. G. A., Vallenari, A., et al. 2016a, *A&A*, 595, A2
 Gaia Collaboration, Prusti, T., de Bruijne, J. H. J., et al. 2016b, *A&A*, 595, A1
 Gaidos, E., Mann, A. W., Lépine, S., et al. 2014, *MNRAS*, 443, 2561
 Gal, R. R., de Carvalho, R. R., Odewahn, S. C., et al. 2004, *AJ*, 128, 3082
 Gillon, M., Triaud, A. H. M. J., Fortney, J. J., et al. 2012, *A&A*, 542, A4
 Girardi, L., Groenewegen, M. A. T., Hatziminaoglou, E., & da Costa, L. 2005, *A&A*, 436, 895
 Gizis, J. E., Reid, I. N., & Hawley, S. L. 2002, *AJ*, 123, 3356
 Górski, K. M., Hivon, E., Banday, A. J., et al. 2005, *ApJ*, 622, 759
 Hawley, S. L., Gizis, J. E., & Reid, N. I. 1997, *AJ*, 113, 1458
 Henden, A., & Munari, U. 2014, *CoSka*, 43, 518
 Henry, T. J., Franz, O. G., Wasserman, L. H., et al. 1999, *ApJ*, 512, 864
 Henry, T. J., & McCarthy, D. W., Jr. 1993, *AJ*, 106, 773
 Hirano, T., Dai, F., Gandolfi, D., et al. 2018, *AJ*, 155, 127
 Høg, E., Fabricius, C., Makarov, V. V., et al. 2000, *A&A*, 355, L27
 Johnson, J. A., & Apps, K. 2009, *ApJ*, 699, 933
 Johnson, J. A., Gazak, J. Z., Apps, K., et al. 2012, *AJ*, 143, 111
 Kaltenegger, L., & Traub, W. A. 2009, *ApJ*, 698, 519
 Kane, S. R., Hill, M. L., Kasting, J. F., et al. 2016, *ApJ*, 830, 1
 Kraus, A. L., Ireland, M. J., Huber, D., Mann, A. W., & Dupuy, T. J. 2016, *AJ*, 152, 8
 Kraus, A. L., Tucker, R. A., Thompson, M. I., Craine, E. R., & Hillenbrand, L. A. 2011, *ApJ*, 728, 48
 Lépine, S., & Gaidos, E. 2011, *AJ*, 142, 138
 Lépine, S., Hilton, E. J., Mann, A. W., et al. 2013, *AJ*, 145, 102
 Lépine, S., Shara, M. M., & Rich, R. M. 2002, *AJ*, 124, 1190
 Mann, A. W., Brewer, J. M., Gaidos, E., Lépine, S., & Hilton, E. J. 2013a, *AJ*, 145, 52
 Mann, A. W., Dupuy, T., Muirhead, P. S., et al. 2017, *AJ*, 153, 267
 Mann, A. W., Feiden, G. A., Gaidos, E., Boyajian, T., & von Braun, K. 2015, *ApJ*, 804, 64
 Mann, A. W., Feiden, G. A., Gaidos, E., Boyajian, T., & von Braun, K. 2016, *ApJ*, 819, 87
 Mann, A. W., Gaidos, E., & Ansdell, M. 2013b, *ApJ*, 779, 188
 Mann, A. W., & von Braun, K. 2015, *PASP*, 127, 102
 Martínez, A. O., Crossfield, I. J. M., Schlieder, J. E., et al. 2017, *ApJ*, 837, 72
 Minkowski, R. L., & Abell, G. O. 1963, in *The National Geographic Society-Palomar Observatory Sky*, ed. K. A. Strand (Chicago, IL: Univ. Chicago Press), 481
 Morton, T. D. 2012, *ApJ*, 761, 6
 Morton, T. D. 2015, VESPA: False Positive Probabilities Calculator, Astrophysics Source Code Library, ascl:1503.011
 Morton, T. D., Bryson, S. T., Coughlin, J. L., et al. 2016, *ApJ*, 822, 86
 Muirhead, P. S., Becker, J., Feiden, G. A., et al. 2014, *ApJS*, 213, 5
 Muirhead, P. S., Edelstein, J., Erskine, D. J., et al. 2011, *PASP*, 123, 709
 Muirhead, P. S., Johnson, J. A., Apps, K., et al. 2012, *ApJ*, 747, 144
 Muirhead, P. S., Mann, A. W., Vanderburg, A., et al. 2015, *ApJ*, 801, 18
 Mukai, K., & Barclay, T. 2018, *Tvguide*, <https://github.com/teessgi/tvguide>, v1.0.0, GitHub
 Neves, V., Bonfils, X., Santos, N. C., et al. 2012, *A&A*, 538, A25
 Newton, E. R., Charbonneau, D., Irwin, J., et al. 2014, *AJ*, 147, 20
 Nutzman, P., & Charbonneau, D. 2008, *PASP*, 120, 317
 Odewahn, S. C., de Carvalho, R. R., Gal, R. R., et al. 2004, *AJ*, 128, 3092
 Reid, I. N., Brewer, C., Brucato, R. J., et al. 1991, *PASP*, 103, 661
 Reid, I. N., Gizis, J. E., & Hawley, S. L. 2002, *AJ*, 124, 2721
 Reid, I. N., Hawley, S. L., & Gizis, J. E. 1995, *AJ*, 110, 1838
 Ricker, G. R. 2014, *JAVSO*, 42, 234
 Ricker, G. R., Winn, J. N., Vanderspek, R., et al. 2015, *JATIS*, 1, 014003
 Rieke, G. H., & Lebofsky, M. J. 1985, *ApJ*, 288, 618

- Rojas-Ayala, B., Covey, K. R., Muirhead, P. S., & Lloyd, J. P. 2012, [ApJ](#), **748**, 93
- Schlaufman, K. C., & Laughlin, G. 2010, [A&A](#), **519**, A105
- Shan, Y., Johnson, J. A., & Morton, T. D. 2015, [ApJ](#), **813**, 75
- Skrutskie, M. F., Cutri, R. M., Stiening, R., et al. 2006, [AJ](#), **131**, 1163
- Stassun, K. G., Kratter, K. M., Scholz, A., & Dupuy, T. J. 2012, [ApJ](#), **756**, 47
- Stassun, K. G., Oelkers, R. J., Pepper, J., et al. 2017, [arXiv:1706.00495](#)
- Sullivan, P. W., Winn, J. N., Berta-Thompson, Z. K., et al. 2015, [ApJ](#), **809**, 77
- Terrien, R. C., Mahadevan, S., Deshpande, R., & Bender, C. F. 2015, [ApJS](#), **220**, 16
- van Leeuwen, F. 2007, [A&A](#), **474**, 653
- West, A. A., Hawley, S. L., Bochanski, J. J., et al. 2008, [AJ](#), **135**, 785
- Winn, J. N. 2010, in *Exoplanets*, ed. S. Seager (Tucson, AZ: Univ. Arizona Press), 55
- Yi, Z., Luo, A., Song, Y., et al. 2014, [AJ](#), **147**, 33
- Zhong, J., Lépine, S., Hou, J., et al. 2015, [AJ](#), **150**, 42